01 Jan 1995

A Flux-weakening Strategy for Current-Regulated Surface-mounted Permanent-magnet Machine Drives

Keith Corzine
Missouri University of Science and Technology

S. D. Sudhoff

H. J. Hegner

A FLUX-WEAKENING STRATEGY FOR CURRENT-REGULATED SURFACE-MOUNTED PERMANENT-MAGNET MACHINE DRIVES

S.D. Sudhoff, Member K.A. Corzine, Student Member
School of Electrical Engineering
University of Missouri - Rolla
Rolla, Missouri 65401

H.J. Hegner, Member
Naval Surface Warfare Center
Annapolis Detachment, Carderock Division
Annapolis, Maryland 21402

Abstract - **Permanent-magnet synchronous machines fed from current-regulated converters feature nearly ideal performance at low-to-moderate speeds. However, as rotor speed increases the back emf rises which results in loss of current regulation and decreased torque. In buried-magnet machine drives, flux weakening is often used to extend the speed range. This paper sets forth a flux-weakening control specifically designed for surface-mounted permanent-magnet machines which is simple and does not require knowledge of the machine or system parameters. The proposed method is demonstrated both experimentally and through the use of computer simulation.**

I. Introduction

Permanent-magnet synchronous machine drives possess many attractive characteristics. In particular, this drive can be made to operate very efficiently, since a permanent magnet supplies the field flux, and at low-to-moderate speeds nearly ideal torque control may be obtained using current-regulated pulse-width-modulated (PWM) converters. There are two varieties of permanent-magnet synchronous machines, buried-magnet machines in which there is pronounced saliency; and surface-mounted-magnet machines in which saliency is not present. The surface-mounted permanent-magnet machine is commonly used and is currently being considered for very high power applications such as ship-propulsion systems.

In either the buried- or surface-mounted permanent-magnet machine drives, if the actual machine currents track the commanded currents the electromagnetic torque tracks the commanded torque, resulting in nearly ideal performance. However, at high speeds the back emf rises which eventually renders the current control ineffective and results in degraded performance.

One method to extend the speed range of a permanent-magnet drive system is to incorporate a PI current control loop in the synchronous reference frame, also called a synchronous current regulator [1]. Such a control will, within the limit set by the maximum possible fundamental component of the output voltage of the converter, guarantee that the fundamental component of the machine current is equal to the commanded current. However, in so doing low-frequency harmonics are introduced which results in low-frequency torque harmonics that may be objectionable in some applications.

Another effective technique to extend the speed range of this class of drives is flux weakening. A variety of flux-weakening controls have been set forth for buried-magnet machines [2-5]. Although these controls cannot be directly used with surface-mounted-magnet machines, at least one author has discussed a feedforward flux-weakening control which can be used [6]. In this paper, a feedback based flux-weakening strategy which does not require knowledge of the machine parameters or dc supply voltage and which is specifically designed for surface-mounted-magnet machines is set forth.

The effectiveness of the proposed control algorithm (referred to as d-axis control) is demonstrated both experimentally and through computer simulation. The performance of an experimental drive system using the proposed d-axis control is compared to the performance of the same system using q-axis control, in which the current command is completely in the q-axis, and to system performance using the synchronous current regulator. Particular emphasis is placed on the time-domain characterization of the controls in order to complement the existing literature, which focuses primarily on torque-speed characteristics.

II. System Description

A 2-pole, 3-phase permanent-magnet synchronous machine is shown in Fig. 1. Therein, each lumped winding actually represents a sinuisodally distributed winding. Mechanical rotor position and speed are denoted θ_{rm} and ω_{rm}, respectively. The electrical rotor position and speed, θ_r and ω_r, are $P/2$ times the corresponding mechanical quantities where P is the number of poles. The electromagnetic and load torques are denoted T_e and T_L. Assuming the machine to be of the surface-mounted-magnet type, to have a sinusoidal back emf, and that the effects of magnetic saturation of the stator iron and eddy currents are negligible, the q- and d- axis voltage equations and torque equation of the permanent-magnet synchronous machine may be expressed in the rotor reference frame as [7]

$$v_{qs}^r = r_s i_{qs}^r + \omega_r(L_{ss} i_{ds}^r + \lambda_m') + L_{ss}\frac{di_{qs}^r}{dt} \quad (1)$$

$$v_{ds}^r = r_s i_{ds}^r - \omega_r L_{ss} i_{qs}^r + L_{ss}\frac{di_{ds}^r}{dt} \quad (2)$$

$$T_e = \frac{3}{2}\frac{P}{2}\lambda_m' i_{qs}^r \quad (3)$$

where r_s, L_{ss}, and λ_m' denote the stator resistance, stator self inductance (the leakage inductance plus 3/2 times the magnetizing

95 WM 065-3 EC A paper recommended and approved by the IEEE Electric Machinery Committee of the IEEE Power Engineering Society for presentation at the 1995 IEEE/PES Winter Meeting, January 29, to February 2, 1995, New York, NY. Manuscript submitted July 22, 1994; made available for printing November 23, 1994.

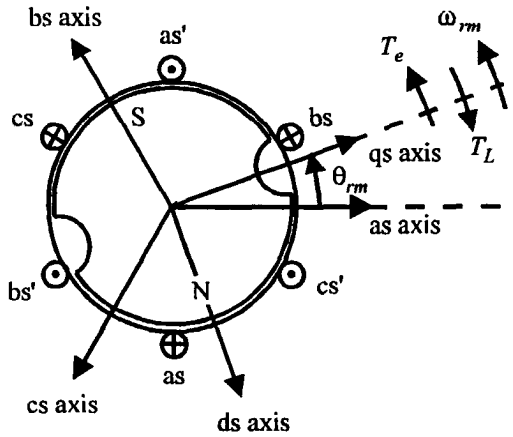

Figure 1. Permanent - magnet synchronous machine.

inductance), and flux linkage due to the permanent magnet, respectively.

In (1-3), the q- and d- axis variables are related to the abc variables by

$$f^r_{qd0s} = K^r_s f_{abcs} \tag{3}$$

where

$$f^r_{qd0s} = \left[\, f^r_{qs} \;\; f^r_{ds} \;\; f^r_{0s} \,\right]^T \tag{4}$$

$$f_{abcs} = \left[\, f_{as} \;\; f_{bs} \;\; f_{cs} \,\right]^T \tag{5}$$

$$K^r_s = \frac{2}{3}\begin{bmatrix} \cos\theta_r & \cos(\theta_r - \frac{2\pi}{3}) & \cos(\theta_r + \frac{2\pi}{3}) \\ \sin\theta_r & \sin(\theta_r - \frac{2\pi}{3}) & \sin(\theta_r + \frac{2\pi}{3}) \\ \frac{1}{2} & \frac{1}{2} & \frac{1}{2} \end{bmatrix} . \tag{6}$$

In (3-5), f may be a voltage, current, or flux-linkage. Henceforth, it will be assumed that the machine is wye-connected whereupon all zero sequence quantities are zero. Although this model cannot be applied to every permanent-magnet synchronous machine it is sufficient to explain the control characteristics which are explored herein. In the event that more detailed analysis techniques are required, the reader is referred to [8-9].

Fig. 2 illustrates a current-regulated permanent-magnet synchronous-machine drive system. In addition to the machine, this system consists of a converter, a supervisory current control, and a hysteresis current control. The inverter consists of six valves, whose gate signals are denoted S_{xy} where 'x' denotes phase and may be 'a', 'b', or 'c', and y denotes the position and is either 'u' if the valve is in the upper half of the bridge or 'l' if the valve is in the lower half. The inverter dc supply voltage is denoted V_{dc} .

The supervisory control determines the current command, i^*_{abcs} , required in order to achieve the commanded torque, T^*_e , based upon the actual stator currents, i_{abcs} , and the electrical rotor position, θ_r . A detailed discussion of various supervisory control strategies is presented in forthcoming sections.

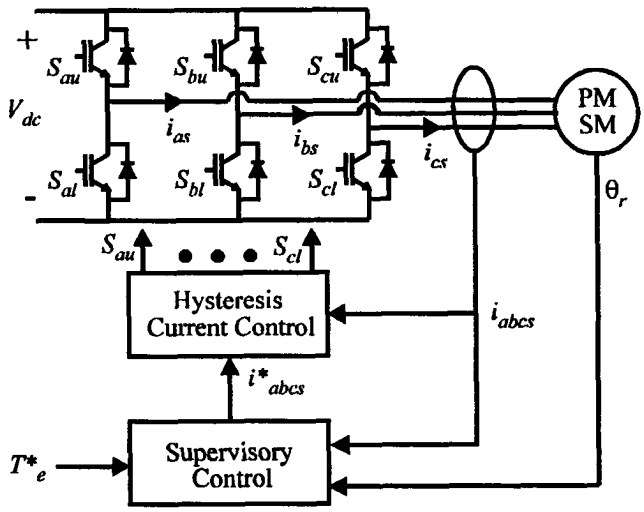

Figure 2. Current regulated brushless dc machine.

Based on the current command i^*_{abcs} and the actual currents i_{abcs} the hysteresis current control depicted in Fig. 3 determines the gate signals to each of the six valves. As can be seen, there are two switching states for each leg, either S_{xu} is on and S_{xl} is off (the positive state), or S_{xu} is off and S_{xl} is on (the negative state), where x may be 'a','b', or 'c'. The parameter h denotes the hysteresis level. If $i_{xs} < i^*_{xs} - h$ and the state of the x'th leg is negative, then a state transition is made to the positive state. Conversely, if $i_{xs} > i^*_{xs} + h$ and the state of the x'th leg is positive, a transition is made to the negative state. Using this type of control with a sufficiently large V_{dc} guarantees that each actual phase current will always be within h of the corresponding commanded phase current. If V_{dc} is not large enough, the phase currents will periodically deviate from the commanded phase currents by an amount greater than h, a condition which is referred to as loss of current tracking.

III. Q-Axis Control

From (3), the q-axis current command corresponding to a torque command T^*_e is given by

$$i^{r*}_{qs} = \frac{2}{3}\frac{2}{P}\frac{T^*_e}{\lambda'_m} . \tag{7}$$

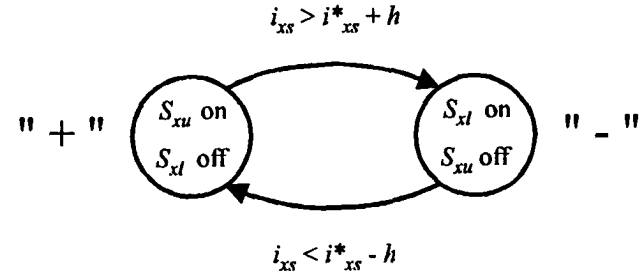

Figure 3. State transition diagram for one leg of hysteresis controlled inverter.

Using this control strategy, the d-axis current command is zero, thus

$$i_{ds}^{r*} = 0 \ . \tag{8}$$

Setting the d-axis current to zero results in maximum torque-per-amp and maximum efficiency. Once the commanded q- and d-axis current commands have been formulated, the abc current command is given by

$$i_{abcs}^{*} = [K_s^r]^{-1} i_{qd0s}^{r*} \tag{9}$$

System performance using q-axis control with a 3A current command at rotor speeds of 1000, 2400, and 2665 rpm is illustrated in Fig. 4a, Fig. 4b, and Fig. 4c, respectively, for an experimental drive whose parameters are listed in the appendix. In each of these figures, the upper trace illustrates the a-phase current measured experimentally, the center trace illustrates the current predicted by a computer simulation, and the third trace illustrates the electromagnetic torque as predicted by the computer simulation. The good correlation between the measured and simulated current waveforms validates the computer simulation, which was used to determine the torque waveform since the equipment necessary for direct measurement was not available.

In the study depicted in Fig. 4a, it can be seen the a-phase current is essentially sinusoidal except for the high frequency switching harmonics. As a result, the electromagnetic torque is nearly constant, and is equal to the commanded torque of 1.40 N•m. However, as speed is increased, the a-phase current periodically deviates from the sinusoidal reference current as illustrated in Fig. 4b. As a result, relatively low frequency harmonics appear in the torque waveform, and the average torque is reduced to 1.13 N•m. As the rotor speed is further increased, the current waveform becomes heavily distorted, as depicted in Fig. 4c. At this speed, the average torque is reduced to 0.51 N•m and torque ripple is even more pronounced.

In order to analytically predict when the loss of current tracking will occur, from (1-2) the commanded q- and d- axis voltages corresponding to the commanded q- and d-axis currents are given by

$$v_{qs}^{r*} = r_s i_{qs}^{r*} + \omega_r (L_{ss} i_{ds}^{r*} + \lambda_m') \tag{10}$$

$$v_{ds}^{r*} = r_s i_{ds}^{r*} - \omega_r L_{ss} i_{qs}^{r*} \ . \tag{11}$$

The peak line-to-neutral voltage which must be supplied by the inverter may be expressed in terms of the q- and d-axis voltages as

$$v_s^* = \sqrt{(v_{qs}^{r*})^2 + (v_{ds}^{r*})^2} \ . \tag{12}$$

Substituting (10-11) into (12) and solving for ω_r yields an expression for the maximum speed for which current tracking, and hence the desired torque, is achieved. In particular,

$$\omega_{r,mx} = \frac{-r_s i_{qs}^{r*} \lambda_m'}{(L_{ss} i_{ds}^{r*} + \lambda_m')^2 + L_{ss}^2 i_{qs}^{r*}} + \frac{\sqrt{r_s^2 \lambda_m'^2 i_{qs}^{r*2} + \left[v_{s,mx}^2 - r_s^2 (i_{qs}^{r*2} + i_{ds}^{r*2})\right]\left[(L_{ss} i_{ds}^{r*} + \lambda_m')^2 + L_{ss}^2 i_{qs}^{r*2}\right]}}{(L_{ss} i_{ds}^{r*} + \lambda_m')^2 + L_{ss}^2 i_{qs}^{r*2}} \tag{13}$$

where $v_{s,mx}$ represents the peak value of v_s which can be supplied by the inverter. To determine $v_{s,mx}$, from Fig. 2 the peak line-to-line voltage the inverter can supply is V_{dc}. Therefore,

$$v_{s,mx} = \frac{V_{dc}}{\sqrt{3}} \tag{14}$$

Using (13-14) indicates that with a q-axis current command of 3 A, the maximum speed at which current tracking, and therefore the

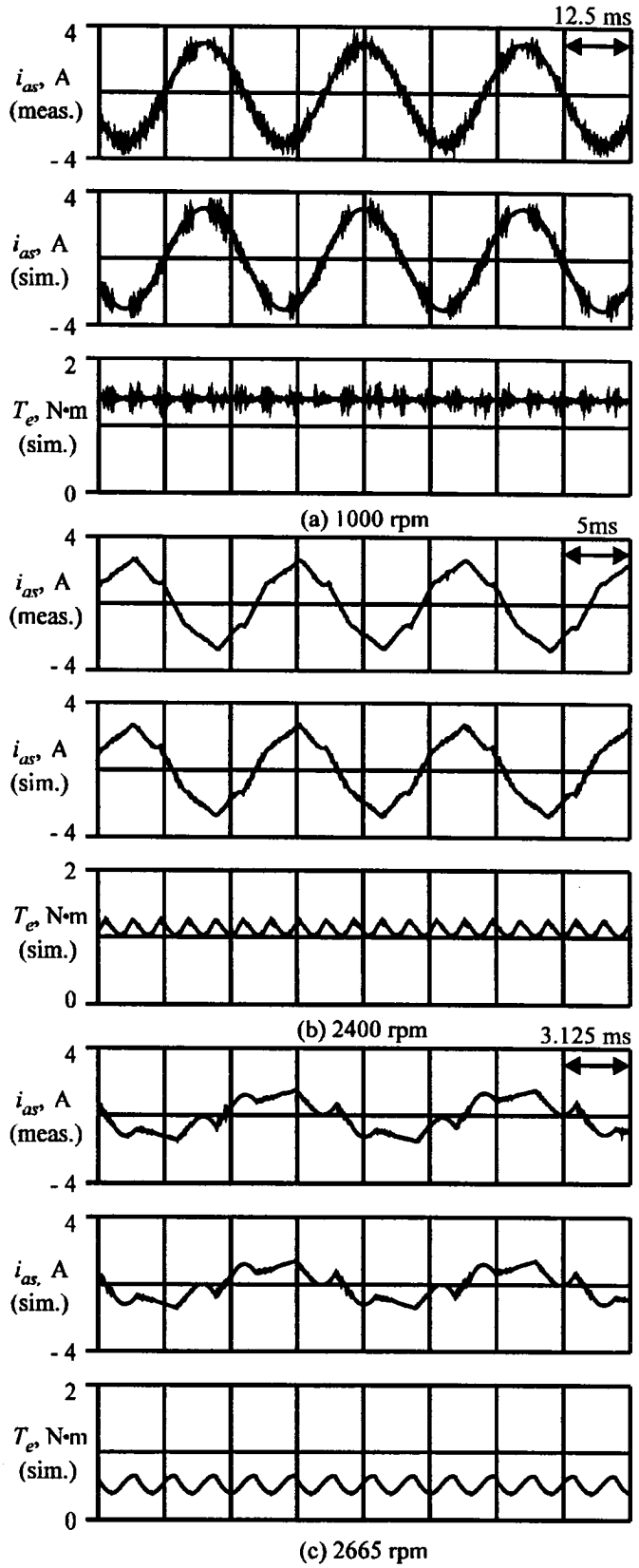

Figure 4. Current and torque waveforms at various rotor speeds using q-axis control.

desired torque, are obtained is 2241 rpm, which is consistent with Fig. 4.

From (14) the most straightforward way to regain current tracking is to increase $v_{s,mx}$ by increasing V_{dc}. However, penalties for doing so include higher semiconductor and capacitor voltage requirements, higher device stresses due to the higher voltage levels, and higher switching frequency at low speeds leading to higher switching losses. To avoid these penalties, a variety of control strategies to extend the speed range without increasing the supply voltage have been proposed.

IV. Synchronous Current Regulator

One method with which to increase the speed range over which the desired torque is achieved without increasing the dc supply voltage is to implement a PI current control loop in the synchronous reference frame (which in this case is identical to the rotor reference frame) as illustrated in Fig. 5. This synchronous current regulator was originally set forth in [1] for current-regulated sine-triangle PWM drives, but is also readily applied to the hysteresis type PWM drive considered herein. In Fig. 5 it is necessary to differentiate between the desired q- and d-axis currents and the current command given to the hysteresis current control loop. Thus i_{qs}^{r*} and i_{ds}^{r*} are the desired values of the q- and d-axis current, while i^{r*}_{qs} and i^{r*}_{ds} are the q- and d-axis currents used to formulate the abc variable current commands, which are comprised of the summation of the desired q- or d-axis current, a term proportional to that axis' current error, and a term proportional to the integral of that axis' current error. The integral term must be limited in order to avoid wind-up in situations where the desired current cannot be achieved.

Due to the integral feedback, the average q- and d-axis currents are equal to their desired value provided the voltage necessary to produce the desired currents does not exceed the maximum fundamental component which can be produced by the inverter. The synchronous current regulator does not extend the range over which the instantaneous currents are tracked; however it does extend the range over which the average value of the commanded q- and d-axis currents are obtained. As a result, the average desired torque is obtained over a larger speed range although the currents in this extended range are distorted resulting in torque ripple.

System performance using the synchronous current regulator is illustrated in Fig. 6. Therein, the same speeds are considered as in Fig. 4, and i_{qs}^{r*} and i_{ds}^{r*} are 3 A and 0 A, respectively. At low speeds (Fig. 6a), operation is essentially identical to the q-axis control, and the electromagnetic torque is essentially constant and equal to its commanded value of 1.40 N•m. As speed is increased (Fig. 6b), current tracking is lost, as in the case of the q-axis control. However, closer examination of Fig. 6b reveals that the peak current is slightly larger than in Fig. 4b due to the integral feedback. As a result, the average q- and d-axis currents are equal to their commanded values, although the instantaneous currents are not. As a result, the average electromagnetic torque using the synchronous current regulator is 1.39 N•m, whereas only 1.13 N•m was obtained using the q-axis control. As the rotor speed is further increased to 2665 rpm (Fig. 6c), the current waveform becomes highly distorted. In this final case the available inverter voltage is insufficient to track

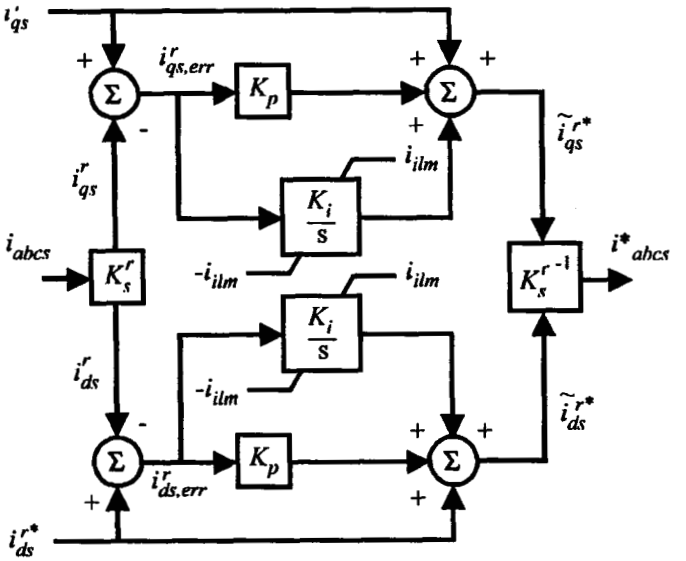

Figure 5. Synchronous current regulator.

even the average value of the commanded current, thus the average torque drops to 0.47 N•m.

The synchronous current regulator is effective as long as the required voltage does not exceed the maximum value of the fundamental component which can be produced by the three-phase bridge in six step mode, i.e.

$$v_{s,mx} = \frac{2}{\pi} V_{dc}. \tag{15}$$

Using (15) to predict the maximum $v_{s,mx}$, and then substituting this value into (13) indicates that with a 3 A q-axis current command the synchronous current regulator is effective to a maximum rotor speed of 2498 rpm, which agrees with Fig. 6.

V. D-Axis Control

Another method to extend the speed range over which nearly ideal performance is obtained is to inject negative current into the d-axis, effectively reducing the back emf of the machine. An expression for the amount of d-axis current which must be injected is found by substituting (14) into (13), replacing $\omega_{r,mx}$ with ω_r, and solving for i_{ds}^{r*}, which yields

$$i_{ds}^{r*} = \frac{-\lambda_m' L_{ss}\,\omega_r^2 + \sqrt{(r_s^2+\omega_r^2 L_{ss}^2)\left(\frac{v_{dc}}{\sqrt{3}}\right)^2 - \left(r_s\lambda_m'\omega_r + (r_s^2+\omega_r^2 L_{ss}^2) i_{qs}^{r*}\right)^2}}{r_s^2+\omega_r^2 L_{ss}^2} \tag{16}$$

D-axis current is injected only when (14) is not satisfied - otherwise the d-axis current command is zero. This type of flux-weakening is similar in effect to flux-weakening in vector controlled induction motor drives except that the magnitude of the d-axis current is increased rather than decreased and that torque production is not affected by the d-axis current injection.

To implement the d-axis current control, (16) could be used directly by a microprocessor. However, this method has a disadvantage in that the parameters of the machine as well as the dc supply voltage must be known. An alternate implementation of this

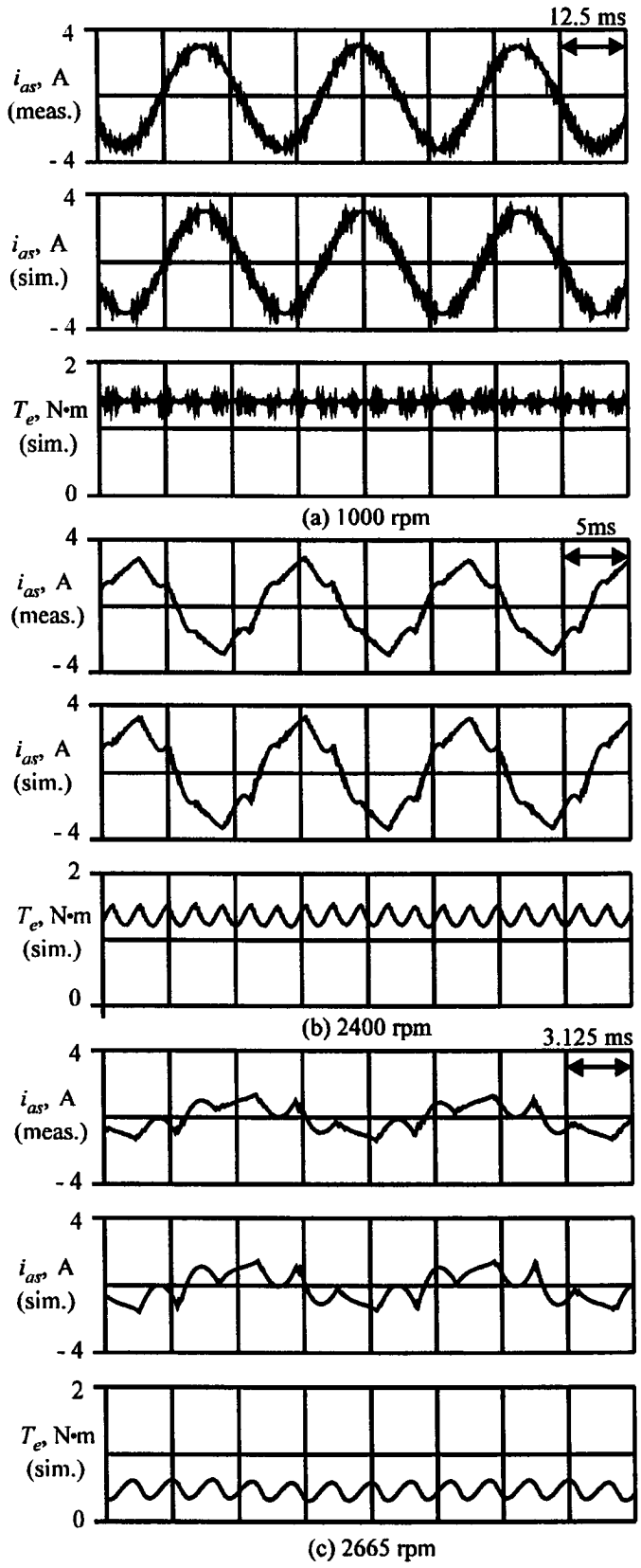

Figure 6. Current and torque waveforms at various rotor speeds using synchronous current regulator.

equation is to use the controller structure shown in Fig. 7, which closely approximates (16) without knowledge of the machine or system parameters.

The control depicted in Fig. 7 consists of several components. The principal part of the control formulates the d-axis current command to the hysteresis current control, i^{r*}_{ds}, which is proportional to the q-axis current error $i^{r}_{qs,err}$. If the q-axis current error is zero, then no d-axis current is injected. If there is a large q-axis current error, then negative d-axis current is injected which lowers the back emf thus improving current tracking, which results in additional q-axis current. Because the feedback is proportional, there will always be some error, but by suitable selection of K_d, the error can be made negligible. The q-axis integral feedback loop (with gain K_i) trims out the small error between the actual q-axis current and commanded q-axis current at low-to-moderate speeds, which prevents d-axis current from being injected unnecessarily. The amount of q-axis current injected due to the integral feedback is limited to i_{tlm} which should be selected to be less than h, the maximum acceptable deviation of the instantaneous current from the commanded phase current. As can be seen in Fig. 7, the d-axis current is limited between 0 and $-i_{dlm}$, where i_{dlm} is a constant, and the q-axis current is limited to values between $-i_{qlm}$ and i_{qlm} where i_{qlm} is determined based on the stator zero-to-peak current limit i_{slm} and the d-axis current command i^{r*}_{ds}.

The advantage of this control rather than programming (16) directly is that knowledge of the machine parameters, dc supply voltage, and rotor speed is not required, and that miscellaneous voltage drops such as semiconductors voltage drops, deadtime in the switching strategy, and current sensor voltage drops are automatically included into the calculation of the d-axis current.

The performance of the d-axis control algorithm is depicted in Fig. 8. At low speed (Fig. 8a), operation is essentially identical to the

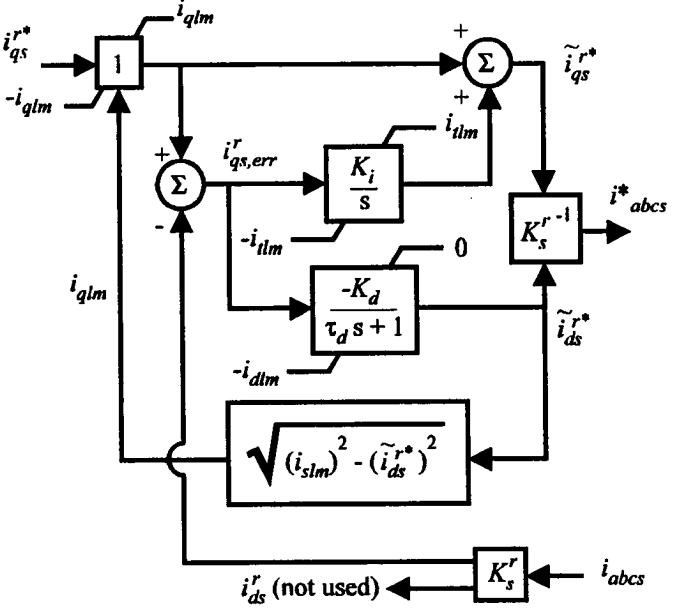

Figure 7. D-Axis control.

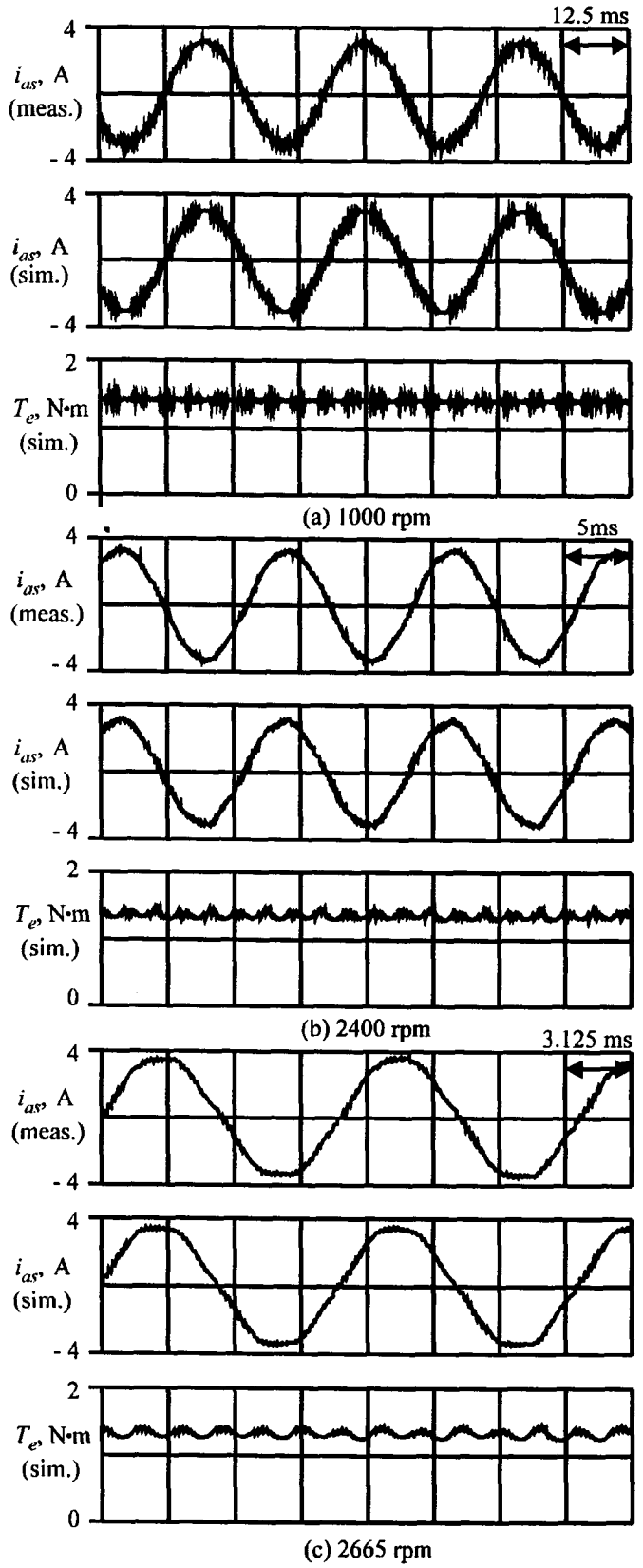

Figure 8. Current and torque waveforms at various rotor speeds using d-axis control.

other methods considered and the commanded torque of 1.40 N•m is obtained. As the speed is increased to 2400 rpm, the electromagnetic torque decreases very slightly to 1.36 N•m. Comparing Fig. 8b to 6b reveals that although the d-axis control maintains the average torque nearly as well as the synchronous current regulator, the currents are essentially sinusoidal and thus the torque ripple is much less than in the case of the synchronous current regulator. At a speed of 2665 rpm, at which the synchronous current regulator becomes ineffective, the d-axis control produces an average torque of 1.33 N•m, with only a slight distortion in the currents and relatively low torque ripple.

A comparison of the amount of d-axis current actually commanded by the control system illustrated in Fig. 7 to that specified by (16) appears in Fig. 9, for a 3 A q-axis current command. As can be seen, the negative d-axis current injection actually starts prior to the speed at which it would be injected according to (16). This is because the semiconductor drops and the switching deadtime necessary to avoid shoot-through tend to have the net effect of decreasing the maximum speed at which current tracking is obtained. As the speed increases, the amount of d-axis current injected becomes lower in magnitude than the ideal amount due to the steady-state error in the d-axis control loop.

The torque-speed curves obtained using the three control strategies described herein are illustrated in Fig. 10. Therein, the solid, dotted, and dashed lines illustrate the electromagnetic torque produced by the q-axis control, synchronous current regulator control (SCR control), and d-axis control, respectively, as calculated by a computer simulation. The box, diamond, and 'x' denote the electromagnetic torque of the three controls as measured experimentally. There is generally good agreement between the average torque predicted by the computer simulation and the measured torque. The discrepancy which does exist is at least in part due to inaccuracy in the torque table used which was operated well below rated torque (56 N•m). As can be seen, the electromagnetic torque begins to fall off at a speed of 2200 rpm in the case of the q-axis control, and at 2400 rpm in the case of the synchronous current regulator. The speeds at which the torque falls off are somewhat less than the predicted values due to the effect of the semiconductor voltage drops. In the case of the d-axis control both the computer simulation and the experimental measurements indicate that the electromagnetic torque is essentially constant over the speed range investigated.

VI. Summary

A method for extending the speed range over which nearly ideal performance of current-regulated surface-mounted permanent-magnet machine drives has been set forth. This method injects the proper amount of d-axis current to insure current tracking without knowledge of the machine parameters or dc supply voltage. The effectiveness of the control was verified both experimentally and using computer simulation. Areas of future research include the modification of the control for both buried-magnet machines and surface-mounted machines with non-sinusoidal back emfs.

VII. Appendix - System Parameters

The parameters of the exterior permanent magnet synchronous machine are $P = 4$, $r_s = 2.98\,\Omega$, $L_{ss} = 11.4$ mH, and $\lambda_m' = 0.156$ Vs. The three-phase bridge converter was operated at

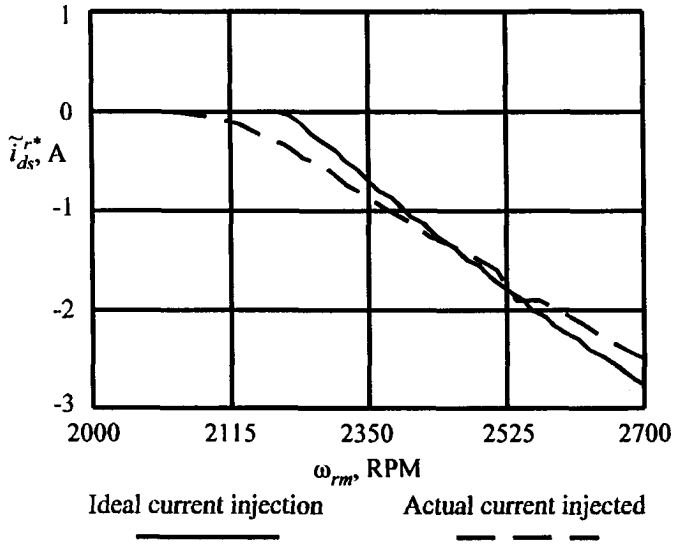

Figure 9. Idealized and actual d-axis current injection.

V_{dc} = 145 V, and h = 0.1 A. The IGBT and diode voltage drops are approximately 1.7 V and 1.0 V, respectively. The IGBT turn on and turn off times are 400 ns and 600 ns, respectively. A switching deadtime of 1.5 μs is used to prevent shoot through. The parameters of the synchronous current regulator are $K_i = 20\ s^{-1}$ and $K_p = 0$. The parameters of the d-axis control are $K_i = 50\ s^{-1}$, $i_{tlm} = 0.05$ A, $K_d = 20.0$, $\tau_d = 50$ ms, $i_{dlm} = 2.5$ A., and $i_{slm} = 5$ A. Both the synchronous current regulator and the d-axis control were implemented digitally with a sampling time of 200 μs.

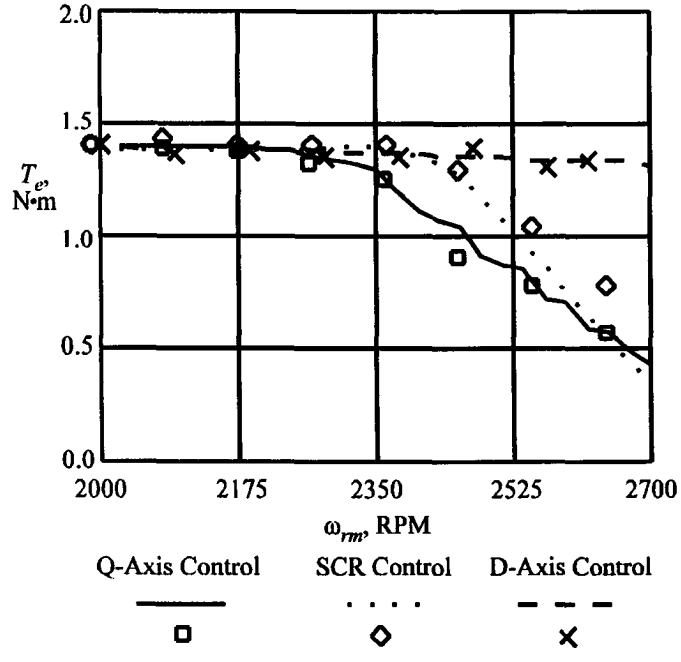

Figure 10. Torque versus speed with various control strategies.

VIII. Acknowledgments

The authors would like to acknowledge support for this project from the Missouri Research Board and the Naval Surface Warfare Center. The authors also extend their gratitude to Dr. Kerkman and Allen-Bradley for the permanent-magnet synchronous machine.

IX. References

[1] T.M. Rowan, R.J. Kerkman, "A New Synchronous Current Regulator and an Analysis of Current-Regulated PWM Inverters," *IEEE Transactions on Industry Applications*, vol. IA-22, no. 4, July/August 1986, pp. 678-690.

[2] S.R. Macminn, T.M. Jahns, "Control Techniques for Improved High-Speed Performance of Interior PM Synchronous Motor Drives," *IEEE Transactions on Industry Applications*, vol. 2, no. 5, September/October 1991, pp. 997-1004.

[3] T.M. Jahns, "Flux-Weakening Regime Operation of an Interior Permanent-Magnet Synchronous Motor Drive," *IEEE Transactions on Industry Applications*, vol. IA-23, no. 4, July/August 1987, pp. 997-1004.

[4] B.K. Bose, "A High Performance Inverter-Fed Drive System of an Interior Permanent Magnet Synchronous Machine," *IEEE Transactions on Industry Applications*, vol. 24, November/December 1988, pp. 987-997.

[5] A.K. Adnanes, T.M. Undeland, "Optimum Torque Performance in PMSM Drives Above Rated Speed," *1991 IEEE Industrial Applications Meeting*, vol. 1, pp. 167-175.

[6] R. Dhaouadi, N. Mohan, "Analysis of Current-Regulated Voltage-Source Inverters For Permanent Magnet Synchronous Motor Drives in Normal and Extended Speed Ranges," *IEEE Transactions on Energy Conversion*, vol. 5 no. 1, March 1990, pp. 987-997.

[7] P.C. Krause, *Analysis of Electric Machinery*, McGraw Hill, 1986.

[8] A.K. Nagarkatti, O.A. Mohammed, and N.A. Demerdash, "Special Losses in Rotors of Electronically Commutated Brushless DC Motors Induced by Non-Uniformly Rotating Armature MMFs," *IEEE Transactions on Power Apparatus and Systems*, vol. PAS-101, December 1982, pp. 4502-4507.

[9] T.W. Nehl, N.A. Demerdash, and F.A. Fouad, "Impact of Winding Inductance's and other Parameters on the Design and Performance of Brushless DC Motors," *IEEE Transactions on Power Apparatus and System*, vol. PAS-104, August 1985, pp. 2206-2213.

Scott D. Sudhoff received the BSEE, MSEE, and Ph.D. degrees at Purdue University in 1988, 1989, and 1991, respectively. He is currently an Assistant Professor at the University of Missouri - Rolla. His interests include the analysis, simulation, and design of electric machinery, drive systems, and finite-inertia power systems. He has authored or co-authored nine journal papers in these areas.

Keith A. Corzine received the BSEE and MSEE degrees from the University of Missouri - Rolla in 1992 and 1994, respectfully, and is currently pursuing the Ph.D. degree. His interests include the design and modeling of electric machinery and electric drive systems.

Henry J. Hegner received the BSEE degree from Virginia Polytechnical Institute and State University in 1983 and MSEE degree from Purdue University in 1992. He is employed within the Electrical Systems Division of the Propulsion and Auxiliaries Department at the Naval Surface Warfare Center, Annapolis, Maryland. He is currently a member of the U.S. Navy's Advanced Surface Machinery Programs where he is serving as Team Leader for the DC Zonal Electrical System Program. For the past 14 years, he has specialized in electrical systems and components for Navy shipboard systems, and has several papers in this area.